HHS Public Access

Author manuscript

Calcif Tissue Int. Author manuscript; available in PMC 2016 March 14.

Published in final edited form as:

Calcif Tissue Int. 2014 May ; 94(5): 484–494. doi:10.1007/s00223-013-9832-5.

Aged Male Rats Regenerate Cortical Bone with Reduced Osteocyte Density and Reduced Secretion of Nitric Oxide After Mechanical Stimulation

Danese M. Joiner,
Orthopaedic Research Laboratories, University of Michigan, Biomedical Science Research Building, 109 Zina Pitcher Place Bay 4888, Ann Arbor, MI 48108, USA

Riyad J. Tayim,
Orthopaedic Research Laboratories, University of Michigan, Biomedical Science Research Building, 109 Zina Pitcher Place Bay 4888, Ann Arbor, MI 48108, USA

John-David McElderry,
Department of Chemistry, University of Michigan, 930 N. University Avenue, Ann Arbor, MI 48108, USA

Michael D. Morris, and
Department of Chemistry, University of Michigan, 930 N. University Avenue, Ann Arbor, MI 48108, USA

Steven A. Goldstein
Orthopaedic Research Laboratories, University of Michigan, Biomedical Science Research Building, 109 Zina Pitcher Place Bay 4888, Ann Arbor, MI 48108, USA

Danese M. Joiner: speededj@med.umich.edu

Abstract

Mechanical loading is integral to the repair of bone damage. Osteocytes are mechanosensors in bone and participate in signaling through gap junction channels, which are primarily comprised of connexin 43 (Cx43). Nitric oxide (NO) and prostaglandin E_2 (PGE_2) have anabolic and catabolic effects on bone, and the secretion of these molecules occurs after mechanical stimulation. The effect of age on the repair of bone tissue after damage and on the ability of regenerated bone to transduce mechanical stimulation into a cellular response is unexplored. The goal of this study was to examine (1) osteocytes and their mineralized matrix within regenerated bone from aged and mature animals and (2) the ability of regenerated bone explants from aged and mature animals to transduce cyclic mechanical loading into a cellular response through NO and PGE_2 secretion. Bilateral cortical defects were created in the diaphysis of aged (21-month-old) or mature (6-month-old) male rats, and new bone tissue was allowed to grow into a custom implant of controlled geometry. Mineralization and mineral-to-matrix ratio were significantly higher in regenerated bone from aged animals, while lacunar and osteocyte density and phosphorylated (pCx43) and total Cx43 protein were significantly lower, relative to mature animals. Regenerated

Correspondence to: Danese M. Joiner, speededj@med.umich.edu.

The authors have stated that they have no conflict of interest.

bone from mature rats had increased pCx43 protein and PGE_2 secretion with loading and greater NO secretion relative to aged animals. Reduced osteocyte density and Cx43 in regenerated bone in aged animals could limit the establishment of gap junctions as well as NO and PGE_2 secretion after loading, thereby altering bone formation and resorption in vivo.

Keywords

Aging; Bone regeneration; Osteocyte; Mechanotransduction; Fragility

Introduction

Bone is a specialized connective tissue that regulates its mass and architecture to meet the daily demands of its external environment [1]. This process is tightly regulated during the repair of damage, which involves replacement of old bone with new bone through osteoclastic bone resorption followed by osteoblastic bone formation [2, 3]. During aging, an imbalance in bone formation and resorption may lead to net bone loss [4]. Mechanical loading on bone influences the activity of cells to deposit, maintain, or remove bone tissue [3]. Osteocytes are the most abundant cells in bone and transduce mechanical cues and communicate with surrounding cells through long cytoplasmic gap junction–coupled processes [3]. Connexin 43 (Cx43), the primary protein in gap junction channels, is an integral component of skeletal development and homeostasis and is involved in the anabolic response to mechanical stimulation [5, 6]. Connexon hemichannels mediate the release of paracrine factors such as prostaglandin E_2 (PGE_2) and nitric oxide (NO) that activate intracellular signaling pathways [5].

PGE_2 is an important mediator in the regulation of bone turnover [7–9]. Local increases in endogenous PGE_2 have been reported during bone healing, but induction of the *COX-2* gene, which is involved in PGE_2 production, is reduced during aging and bone repair [10, 11]. Mechanical stimulation also produces rapid transient increases in NO, which can inhibit bone resorption and increase PGE_2 release by osteocytes [12]. Low doses of NO can inhibit bone-resorbing activity or activate bone formation, but high levels of NO can cause bone resorption through inflammatory mechanisms [13, 14]. NO synthesis plays an important role in bone healing, and differential modulation of NO synthase with age has been reported in a variety of tissue types [15–18].

Physiologic loading is important for preserving tissue integrity and during remodeling repair [1, 19]. Age may affect the transduction of mechanical stimulation into an anabolic response within bone tissue, but there are conflicting data in the literature. Some animal models suggest that age reduces the anabolic response of bone to mechanical stimulation, but other models have shown no differences with age or an increased responsiveness in aged animals [20–25]. Both an anabolic response to exercise and no change have been reported in older humans relative to control groups [26, 27]. The effects of age on the repair of bone tissue after damage and on the ability of regenerated bone tissue to transduce mechanical stimulation into a cellular response are unexplored. The goal of this study was to examine (1) osteocytes and their mineralized matrix within regenerated bone from aged and mature

animals and (2) the ability of regenerated bone explants from aged and mature animals to transduce cyclic mechanical loading into a cellular response through NO and PGE_2 secretion. We studied osteocytes within their native three-dimensional mineralized environment, through which they perceive physical stimuli, using custom hardware developed in our laboratory [28]. A reduction in cortical bone osteocyte density has previously been reported during aging; therefore, we hypothesized that aged animals would produce regenerated bone explants with lower osteocyte density and lower Cx43 relative to mature animals. Furthermore, explants from aged animals would have a reduced response to mechanical stimulation through NO and PGE_2 secretion.

Materials and Methods

The Institutional Animal Care and Use Committee at the University of Michigan approved all experimental procedures.

Animals

There is no commercially available instrumentation to produce and mechanically load regenerated bone specimens of controlled geometry. Therefore, we used custom implant hardware developed earlier in our laboratories within which new bone could be grown and then later removed from the animal for analysis. Sixteen mature (6 months old) and 18 aged (21 months old) male Sprague-Dawley rats were purchased from Zivic Laboratories (Portersville, PA, USA) and bilaterally fitted with the custom implant [28]. The implant consisted of a channel plate ($2.49 \times 3.15 \times 0.51$ mm^3) with two open parallel channels (794 μm wide × 254 μm deep) shaped like dumbbells, plus a $14 \times 4 \times 0.25$ mm^3 cover plate (Fig. 1a) [28].

Animals were anesthetized using 2 % isoflurane; they then received 5 mL of warmed lactated Ringer's solution mixed with butorphenol (1 mg/kg), followed by atropine (0.1 mg/kg) subcutaneously. After the lower extremities were prepared for aseptic surgery, the anterolateral femoral diaphysis was exposed through a lateral 2-cm parallel incision. After elevating the periosteum, a 254-μm-deep, rectangular (2.49×3.15 mm^2) femoral cortical defect was created with a dental burr (Sullivan-Schein Dental, West Allis, WI, USA) (Fig. 1b). The dimensions were verified with a custom template. Implants were fitted to the diaphysis, with the channel plate suspended in the defect and the cover plate resting on the periosteal surface; the implant was stabilized (after predrilling) with self-tapping screws (Fig. 1c). The procedure was repeated in the contralateral femora. One 6-month old rat and three 21-month-old rats died postoperatively; thus, 15 mature and 15 aged rats were used for analyses.

The implantation periods were selected based on data from a previous study using the implant in our laboratory on 51 6-month-old male Sprague-Dawley rats. These data suggested that, on average, maximum bone volume fraction and bone mineral density (BMD) were reached after 12 weeks [28]. Thus, following a 3-month ($n = 5$ mature and $n = 5$ aged) or a 4-month ($n = 10$ mature and $n = 10$ aged) implantation period, animals were anesthetized and the implant hardware was removed under sterile conditions. After implant removal from both limbs, animals were killed intraoperatively with 100 mg/kg intracardiac

sodium pentobarbital. Whole femora from mature (n = 10) and aged (n = 10) animals used for 4-month implantation studies were also harvested, to examine native cortical bone from these animals. Tissue characterization experiments used independent, randomly selected, regenerated specimens from mature animals (n = 6) and from aged animals (n = 8). For the mechanical loading experiments, we randomly selected two specimens from the same animal and designated one as sham-treated and the other as loaded (n = 11 sham-treated, n = 11 loaded specimens from mature animals, n = 9 sham-treated and n = 9 loaded specimens from aged animals).

The channel plate containing the regenerated bone explant was extracted en bloc with a custom elevator and placed in serum-free BGJb (Fritton-Jackson modification) culture medium. Tissue explants were removed from the channels, transferred to a Petri dish containing growth medium (BGJb with 10 % heat-inactivated fetal bovine serum, 100 U/mL penicillin, 100 μg/mL streptomycin, and 5 μg/mL amphotericin B), and incubated at 37 °C with 5 % CO_2 plus 75 μg/mL daily ascorbic acid. All tissue culture products were purchased from Invitrogen (Carlsbad, CA, USA).

Characterization of Regenerative Bone Explants and Femora

Micro-computed Tomography—Regenerated explants were scanned on a commercially available micro-computed tomographic (microCT) system with a source voltage of 80 kVp (eXplore Locus; GE Healthcare Pre-Clinical Imaging, London, Canada). Specimens were immersed in distilled water, and an acrylic beam flattener was used to equalize the beam path length within the field of view. The scan setup used a magnification of 2.60 with 2 × 2 detector binning, which resulted in an acquired pixel size of 18 μm. In each scan, 720 projections were acquired over 360° of rotation. The projections were corrected using low-end and high-end outlier replacement in conjunction with a sonogram-based, long-term trend correction, and they were reconstructed using a filtered cone beam back-projection algorithm with a Ram-Lak filter to generate images with an isotropic voxel size of 18 μm (Fig. 1d). Calibration was performed with a phantom containing air, water, and SB3. Data were thresholded to binary images of bone and nonbone voxels, which were extrapolated from air and water Hounsfield units.

The region of interest (ROI) was created with the cortical tool, which selects an ROI corresponding to the cortical shell of bone and uses a series of morphological operators to semiautomatically select cortical bone components. A gray-level threshold value (obtained from histograms of average gray-scale value and frequency) and two scaling size parameters were used to separate out cortical bone voxels and improve the accuracy of the ROI tool. BMD was calculated [29]. Whole femora were cleaned of soft tissue and scanned using the same settings but reconstructed onto 45-μm voxels. Cortical geometric analyses were performed for cortical thickness, cross-sectional area, bending moment of inertia for the medial– lateral axis (Iyy), BMD, inner fiber length (distance from the center of the medullary canal to the endosteal surface), and outer fiber length (distance from the center of the medullary canal to the periosteal surface) on a 3-mm mid-diaphyseal femoral segment, as described previously [30]. The cortical segment did not include the region used to generate microspecimens.

Histology—Femora and regenerated explant specimens were fixed for 48 h in 10 % neutral-buffered formalin, decalcified in formic acid/sodium citrate solution, and processed for 24 h in graded alcohols and xylene prior to paraffin embedding. Tissue was sectioned at 7 μm and stained with alcian blue (1 g alcian blue in 100 mL 3 % acetic acid) and hematoxylin (1.5 g hematoxylin in 250 mL distilled H_2O). Slides were alcohol-dehydrated, cleared, mounted, and imaged at 40× with a Carl Zeiss MicroImaging light microscope (Jena, Germany). Lacunae and osteocytes were counted on an average of 26 and 22 slides per sample from mature and aged animals, respectively, and normalized to bone area to calculate lacunar and osteocyte density. Immunofluorescence was performed on femoral sections for cleaved caspase-3 to examine apoptosis (Cell Signaling Technology, Danvers, MA, USA; 1:300) according to the manufacturer's instructions. The area of cleaved caspase-3 staining was quantified and normalized to bone area with Image J software (National Institutes of Health, Bethesda, MD, USA).

Raman Spectroscopy—Femoral and regenerated explant specimens were also analyzed by Raman spectroscopy. The Raman imaging system consisted of a 785-nm diode laser (Kaiser Optical Systems, Ann Arbor, MI, USA) guided through an upright fluorescence microscope (Eclipse ME600; Nikon Instruments, Melville, NY, USA) functioning in reflection mode. Scattered light was collected through a 20*x*/0.75NA objective (Super Fluor series, Nikon Instruments) and an imaging spectrometer (HoloSpec f/1.8i, Kaiser Optical Systems) before being imaged onto a back-illuminated deep depletion CCD camera (Classic; Andor Technology, South Windsor, CT, USA). The CCD image was treated as a multichannel detector acquiring about 100 spectra simultaneously and averaging them into one spectrum for increased signal-to-noise ratio. Spectral bands in the 800–1,015 cm^{-1} region were fit to gaussian–Lorentzian functions using a nonlinear least squares algorithm. The bone development metrics mineral-to-matrix ratio and crystallinity were measured as the ratio of the phosphate 960 cm^{-1} band to the phenylalanine 1,001 cm^{-1} band and as the phosphate 960 cm^{-1} inverse bandwidth, respectively [31].

Osteopontin Quantification—Osteopontin is an abundant noncollagenous sialoprotein in the bone matrix and plays a role in osteoclast attachment and resorption. Osteopontin stimulates bone formation in vitro and may mediate cell–cell interactions via integrin binding; therefore, it was assessed [32]. After 3 days of culture, the medium was collected adjacent to regenerated explant specimens and assayed with an osteopontin (rodent) EIA kit from Assay Designs (Ann Arbor, MI, USA) according to the manufacturer's instructions. Background optical density was subtracted from all specimens, and a calibration curve was constructed from which a sample osteopontin concentration could be determined. Osteopontin concentration was normalized to explant protein concentration, which was determined by BCA (Thermo Scientific, Rockford, IL, USA).

Mechanical Loading of Regenerative Bone Explants

Three-Point Bending—A custom three-point bending apparatus allowed the tissue to be maintained in serum-free culture medium (1 mL) and in an incubator (37 °C and 5 % CO_2) while being mechanically loaded (Fig. 1e). The loading device was driven by a linear motor controlled by APT software (www.aptsoftware.com) and connected to a load cell.

Regenerated explants were cyclically loaded at a 0.5 μm/second (0.02 Hz) rate for a total of 60 min to a maximum displacement of 14 μm; the loading parameters were scaled from a protocol used on larger bone explants [33]. Specimens were loaded along a gauge length of 1,245 μm, and no indentations of the regenerated bone occurred as a result of the center load. In sham treatment, explant specimens were placed in the loading device, immediately removed, and placed in 1 mL of serum-free medium within a culture dish and into the incubator. Medium (250 μL) was harvested from each loaded and sham sample at a location adjacent to the tissue after 15, 30, 45, and 60 min. Specimens were snap-frozen in 1× PBS and stored at −80 °C after 60 min of treatment until protein extraction and quantification.

PGE_2 and NO Concentration—Medium from sham and loaded specimens was assayed in triplicate using a PGE_2 EIA kit and an NO colorimetric kit from Cayman Chemical (Ann Arbor, MI, USA), according to the manufacturer's instructions. To quantify PGE_2, 50 μL of medium was added to each well of a microplate coated with PGE_2 antibody. PGE_2 AChE tracer and monoclonal antibody were added to wells and incubated at 4 °C for 18 h. After incubation, wells were washed five times with wash buffer and then incubated at room temperature for 90 min in the dark with Ellman's reagent. The plate was read at 420 nm on a Spectra Max v5 plate reader (Molecular Devices, Sunnyvale, CA, USA). To calculate NO concentration, 30 μL of medium was added to each well of a microplate. Enzyme cofactor mixture (10 μL) and nitrate reductase mixture (10 μL) were added to the wells, and the plate was incubated for 2.5 h at room temperature. Following incubation, Griess reagent 1 (10 μL) followed by Griess reagent 2 (10 μL) were added to the wells, and after 10 min the plate was read at 550 nm on a Spectra Max v5 plate reader (Molecular Devices). Background optical density was subtracted from all specimens, and a calibration curve was constructed from which sample PGE_2 and NO concentrations could be determined. PGE_2 and NO concentrations were normalized to explant protein concentration, which was determined by BCA.

Western Blot—Sham-treated and mechanically loaded, regenerated explants were homogenized in lysis buffer (96 % RIPA buffer, 1 % sodium orthovanadate, 1 % phenylmethanesulfonyl fluoride, 2 % protease inhibitor cocktail; Santa Cruz Biotechnology, Santa Cruz, CA, USA) and protein was quantified with BCA. Equal amounts of protein from each sample (10 μg) were loaded into the lanes of a 10 % Tris-HCl acrylamide gel with 25 μL of 2× electrophoresis sample buffer (Santa Cruz Biotechnology) and subjected to SDS-PAGE. The proteins were then transferred to a PVDF membrane and blocked in 5 % blotto (5 % powdered milk in Tris-buffered saline plus 1 % Tween-20) overnight at 4 °C. After blocking, membranes were washed and incubated overnight at 4 °C with primary antibodies against phosphorylated Cx43 (pCx43; 1:1,000), total Cx43 (1:100,000), and GAPDH (1:1,000). Membranes were then washed and probed with horseradish peroxidase-conjugated anti-rabbit secondary antibody for 1 h at room temperature. Finally, membranes were washed, developed with ECL (Thermo Scientific), and quantified by densitometry using Image J software. Antibodies were purchased from Abcam (Cambridge, MA, USA) and Cell Signaling Technology.

Statistical Analysis

GraphPad Prism software (GraphPad, La Jolla, CA, USA) was used for statistical analysis. We assessed normality with a D'Agostino-Pearson omnibus normality test and used the ROUT method to determine outliers. NO and PGE_2 data contained extreme outliers, which were removed from the analysis. NO and PGE_2 data were not normally distributed; therefore, we used a Kruskal-Wallis and Dunn multiple comparisons test on NO and PGE_2 measurements. A two-way analysis of variance was used to determine statistical significance for all other data. There was no significant difference due to implantation time; therefore, the average and SD were calculated from the combined data of both implantation periods for each age group. *p* values were considered statistically significant at the 0.05 level.

Results

Callous formation did not occur during healing, and the percentages of the implanted chambers that were partially filled (mature = 22.5 ± 21.9, aged = 30 ± 23) or completely filled (mature = 62.5 ± 17.7, aged = 60 ± 33.7) were not significantly different between age groups. Regenerated explant mineral density was significantly higher for aged animals ($p < 0.05$), as was the mineral-to-matrix ratio ($p < 0.05$) (Fig. 2a, b). For aged rats (relative to mature rats), the native femoral cortical BMD, cross-sectional area, inner fiber length, outer fiber length, and bending moment of inertia were significantly greater ($p < 0.01$); but cortical thickness was not (Table 1). Femur crystallinity was significantly lower ($p < 0.01$) for aged animals (mature = 0.0626 ± 0.0004, aged = 0.0617 ± 0.0006) (Fig. 2c), but there was no significant difference in femur mineral-to-matrix ratio (mature = 11.96 ± 4.84, aged = 11.67 ± 4.08) or in regenerated explant crystallinity (mature = 0.054 ± 0.002, aged = 0.053 ± 0.001) between groups. Secreted osteopontin concentration from regenerated explants was significantly higher for aged animals ($p < 0.01$) (Fig. 2d).

Lacunae were present in regenerated explant specimens from both mature and aged rats; tissue from aged animals appeared more woven and disorganized, with fewer osteocytes within lacunae (Fig. 3a). The regenerated explant lacunar density was significantly lower ($p < 0.01$) for aged rats, as was the osteocyte density ($p < 0.01$) (Fig. 3b, c). There was no qualitative difference between groups in cortical femoral cell morphology, but lacunar density in femora was significantly lower ($p < 0.01$) for aged animals (Fig. 3a, b). There was no statistically significant difference in femoral osteocyte density between groups (Fig. 3c). Lacunar density was significantly lower in regenerated explants from both mature ($p < 0.01$) and aged ($p < 0.01$) animals relative to femoral cortical bone from the respective age groups (Fig. 3b). Osteocyte density was significantly lower ($p < 0.01$) in regenerated explants from aged animals relative to that in femoral cortical bone (Fig. 3c). The effect of age on osteocyte density in regenerated explants and femoral cortical bone was significantly different (interaction $p < 0.0001$) (Fig. 3c). We also observed a significant increase ($p < 0.05$) in cleaved caspase-3 staining in femoral cortical bone near the defect in aged relative to mature animals (Fig. 3d, e).

pCx43 protein was significantly lower ($p < 0.01$) in sham-treated and loaded ($p < 0.01$), regenerated explants from aged relative to mature animals (Fig. 4a, b). pCx43 increased significantly ($p < 0.01$) in regenerated explants from mature animals with mechanical

loading (Fig. 4a, b). The effect of load on pCx43 in regenerated explants was significantly different in mature and aged animals (interaction $p < 0.05$) (Fig. 4b). Total Cx43 protein levels were significantly lower in both sham-treated ($p < 0.01$) and loaded ($p < 0.01$), regenerated explants from aged rats than in regenerated explants from mature rats (Fig. 4a, c). We studied the concentration of NO and PGE_2 in sham-treated and mechanically loaded, regenerated explants from both age groups. NO was significantly lower ($p < 0.01$) for sham-treated and loaded, regenerated explants from aged animals relative to mature loaded, regenerated explants after 15, 30, and 45 min (Table 2). NO concentrations were significantly different between mature sham, mature loaded, aged sham, and aged loaded groups at 15 min (Kruskal-Wallis $p < 0.001$), 30 min (Kruskal-Wallis $p < 0.001$), 45 min (Kruskal-Wallis $p < 0.01$), and 60 min (Kruskal-Wallis $p < 0.05$) (Table 2). PGE_2 was significantly greater for loaded, regenerated explants from mature animals relative to sham after 60 min ($p < 0.05$); and at this time point PGE_2 concentrations were significantly different between mature sham, mature loaded, aged sham, and aged loaded groups (Kruskal-Wallis $p < 0.05$) (Table 3).

Discussion

The role of mechanical loading at the molecular level in regenerated bone in aging animals remains largely unexplored. We examined osteocytes and the mineralization of regenerated bone produced in aged and mature animals. We also examined the ability of regenerated bone from aged and mature rats to transduce cyclic mechanical stimulation into a cellular response through PGE_2 and NO secretion. We found that bone regeneration was similar between the two age groups. Others have reported a delay in the healing of larger defects with increased age, an increase in non-unions, and reduced removal of microcracks after load-induced damage [11, 34]. We found that bone regeneration was similar between the two age groups, which could be attributed to the mechanism of bone formation (which was primarily intramembranous), the stability provided by our implant hardware, and controlled-defect geometry [28].

Mineralization provides strength and stiffness to the bone, but excessive mineralization can have a negative effect on bone ductility [35–37]. Increased mineralization can cause bone to become brittle, reducing the energy required for fracture [38]. In aged mice an increase in femoral mineral-to-matrix ratio, which positively correlates with the plastic index and is negatively associated with hardness and creep viscosity, has been reported [39]. There are also reports in aged mice of increased crystallinity, which is correlated positively with tissue-level strength and stiffness and negatively with deformation [39, 40]. In this study, regenerated bone from aged animals had increased mineralization and a higher mineral-to-matrix ratio. Femoral cortical BMD and geometric properties were also increased in aged animals, consistent with previous studies [39, 41]. We observed no difference between age groups in the crystallinity of regenerated bone, which is consistent with human data; but we found reduced crystallinity and no difference in mineral-to-matrix ratio within femoral cortical bone with age. Differences between our results and those of others may be due to differences in the animal model and ages used in the experiments [40]. Increased mineralization may reduce deformation, local strain, and the mechanical stimuli to

osteocytes, thereby influencing the cellular transduction of mechanical stimulation in regenerated bone.

Increased mineralization in regenerated bone from aged animals may be due to accelerated cellular mineralization and/or osteoblast differentiation, but several studies have shown either no difference or impaired or delayed osteoprogenitor cell differentiation with aging [42, 43]. The ability of osteocytes to alter the composition of their extracellular matrix has been reported [44]. An increase in the number of highly mineralized osteocyte lacunae within the periosteal and endocortical regions of femora has been observed with increased age, which is consistent with the significantly higher mineralization of regenerated explants and cortical bone from aged animals (relative to mature) observed in our study [42, 44]. Osteocyte apoptosis is stimulated by a variety of factors including microdamage, and the death of these cells can induce lacunar hypermineralization, leading to brittleness and susceptibility to microdamage [44]. We observed increased cleaved caspase-3 in femoral cortical bone near the defect in aged animals relative to mature; therefore, osteocyte apoptosis might reduce cell density in regenerated bone from aged animals and contribute to increased mineralization.

Studies have reported an exponential decline in osteocyte lacunar density with age in the cortical bone of the femoral mid-diaphysis, as well as significant decreases in osteocyte lacunar density within the periosteal and endocortical regions of femora from males and females [44, 45]. We found that regenerated bone from aged rats had reduced osteocyte and lacunar density and that femoral cortical bone from aged rats had reduced lacunar density. Significantly fewer osteocyte lacunae have been reported in the area adjacent to microcracks relative to peripheral areas, which is consistent with our observation of significantly lower lacunar density in regenerated bone relative to corresponding femoral cortical bone for both age groups [44]. Osteocyte density was significantly lower in regenerated bone relative to femoral cortical bone from aged (but not from mature) animals. Aged animals were not able to regenerate bone that recapitulated the cell density of native cortical bone, an inability that could reduce cell communication and signaling and increase the susceptibility to further damage and fracture.

The effects of Cx43, NO, and PGE_2 on bone during normal and pathological conditions, as well as changes in the expression of these molecules after mechanical stimulation, have been well documented. Mechanical stimulation can induce rapid and transient increases in NO and PGE_2 concentration and can increase Cx43 and gap junction intracellular communication in several cell types [28–34]. We found that regenerated bone explants from aged animals had lower amounts of NO secreted after loading relative to mature animals and no change in PGE_2 secretion after loading. However, in mature animals pCx43 and total Cx43 protein levels were higher in both sham-treated and loaded, regenerated explants; and there was an increase in explant pCx43 protein and PGE_2 secretion with 60 min of loading. Others have observed an increase in Cx43 for up to 16 h of applied mechanical loading; thus, the maximum time point of 60 min in our experiments may not have allowed us to detect an increase in Cx43 after loading in regenerated bone [46]. Less Cx43 protein in regenerated bone from aged animals is likely the result of lower osteocyte density, which could decrease cell communication and the ability to transduce mechanical stimulation into

a cellular response through PGE_2 secretion as well as result in a lower secretion of NO. Differences in NO and osteopontin secretion between the two age groups could affect both bone formation and resorption in vivo but were not fully elucidated in this study.

During aging, an imbalance in bone formation and resorption may occur, leading to net bone loss [4]. It has been hypothesized that whole-bone failure in osteoporosis may be a result of positive feedback between microdamage and the resulting remodeling that attempts to repair the damage [34]. Increased mineralization, reduced cell density, and reduced amount of Cx43 in regenerated bone, as well as unaltered PGE_2 and reduced secretion of NO after mechanical stimulation, may also be involved. Increased mineralization could decrease local deformation, and the reduced number of osteocytes and amount of Cx43 could limit the ability of regenerating bone in aged rats to establish gap junctions and secrete NO and PGE_2 in response to mechanical loading. Reduced NO secretion could alter both bone formation and resorption in vivo, which could contribute to the imbalance between resorption and formation in aging animals and affect the risk of fragility fractures.

Acknowledgments

The authors thank XiXi Wang, Sharon Reske, Kathy Sweet, and Bonnie Nolan for animal care; Dennis Kayner and Charles Roehm for their assistance with the three-point bending system; and David Nadziejka for technical editing of the manuscript. An NSF Graduate Student Research Fellowship (D.M.J.) and NIH grant R01 AR51504 (S.A.G.) supported this work.

References

1. Rubin CT, Lanyon LE. Regulation of bone formation by applied dynamic loads. J Bone Joint Surg Am. 1984; 66(3):397–402. [PubMed: 6699056]
2. Raggatt LJ, Partridge NC. Cellular and molecular mechanisms of bone remodeling. J Biol Chem. 2010; 285(33):25103–25108. [PubMed: 20501658]
3. Robling AG, Castillo AB, Turner CH. Biomechanical and molecular regulation of bone remodeling. Annu Rev Biomed Eng. 2006; 8:455–498. [PubMed: 16834564]
4. Szulc P, Garnero P, Munoz F, Marchand F, Delmas PD. Cross-sectional evaluation of bone metabolism in men. J Bone Miner Res. 2001; 16(9):1642–1650. [PubMed: 11547833]
5. Loiselle AE, Jiang JX, Donahue HJ. Gap junction and hemichannel functions in osteocytes. Bone. 2013; 54:205–212. [PubMed: 23069374]
6. Stains JP, Civitelli R. Gap junctions in skeletal development and function. Biochim Biophys Acta. 2005; 1719(1–2):69–81. [PubMed: 16359941]
7. Blackwell KA, Raisz LG, Pilbeam CC. Prostaglandins in bone: bad cop, good cop? Trends Endocrinol Metab. 2010; 21(5):294–301. [PubMed: 20079660]
8. Weinreb M, Rutledge SJ, Rodan GA. Systemic administration of an anabolic dose of prostaglandin E_2 induces early-response genes in rat bones. Bone. 1997; 20(4):347–353. [PubMed: 9108355]
9. Gao Q, Xu M, Alander CB, Choudhary S, Pilbeam CC, Raisz LG. Effects of prostaglandin E_2 on bone in mice in vivo. Prostaglandins Other Lipid Mediat. 2009; 89(1–2):20–25. [PubMed: 19464663]
10. Dekel S, Lenthall G, Francis MJ. Release of prostaglandins from bone and muscle after tibial fracture: an experimental study in rabbits. J Bone Joint Surg Br. 1981; 63-B(2):185–189. [PubMed: 7217139]
11. Naik AA, Xie C, Zuscik MJ, Kingsley P, Schwarz EM, Awad H, et al. Reduced COX-2 expression in aged mice is associated with impaired fracture healing. J Bone Miner Res. 2009; 24(2):251–264. [PubMed: 18847332]

12. Chow JW, Fox SW, Lean JM, Chambers TJ. Role of nitric oxide and prostaglandins in mechanically induced bone formation. J Bone Miner Res. 1998; 13(6):1039–1044. [PubMed: 9626636]
13. van't Hof RJ, Ralston SH. Nitric oxide and bone. Immunology. 2001; 103(3):255–261. [PubMed: 11454054]
14. Damoulis PD, Hauschka PV. Nitric oxide acts in conjunction with proinflammatory cytokines to promote cell death in osteoblasts. J Bone Miner Res. 1997; 12(3):412–422. [PubMed: 9076584]
15. Zhu W, Diwan AD, Lin JH, Murrell GA. Nitric oxide synthase isoforms during fracture healing. J Bone Miner Res. 2001; 16(3):535–540. [PubMed: 11277271]
16. Diwan AD, Wang MX, Jang D, Zhu W, Murrell GA. Nitric oxide modulates fracture healing. J Bone Miner Res. 2000; 15(2):342–351. [PubMed: 10703937]
17. Baldik Y, Diwan AD, Appleyard RC, Fang ZM, Wang Y, Murrell GA. Deletion of iNOS gene impairs mouse fracture healing. Bone. 2005; 37(1):32–36. [PubMed: 15894526]
18. Cau SB, Carneiro FS, Tostes RC. Differential modulation of nitric oxide synthases in aging: therapeutic opportunities. Front Physiol. 2012; 3:218. [PubMed: 22737132]
19. Waldorff EI, Christenson KB, Cooney LA, Goldstein SA. Microdamage repair and remodeling requires mechanical loading. J Bone Miner Res. 2010; 25(4):734–745. [PubMed: 19821772]
20. Turner CH, Takano Y, Owan I. Aging changes mechanical loading thresholds for bone formation in rats. J Bone Miner Res. 1995; 10(10):1544–1549. [PubMed: 8686511]
21. Donahue SW, Jacobs CR, Donahue HJ. Flow-induced calcium oscillations in rat osteoblasts are age, loading frequency, and shear stress dependent. Am J Physiol Cell Physiol. 2001; 281(5):C1635–C1641. [PubMed: 11600427]
22. Rubin CT, Bain SD, McLeod KJ. Suppression of the osteogenic response in the aging skeleton. Calcif Tissue Int. 1992; 50(4):306–313. [PubMed: 1571841]
23. Silbermann M, Bar-Shira-Maymon B, Coleman R, Reznick A, Weisman Y, Steinhagen-Thiessen E, et al. Long-term physical exercise retards trabecular bone loss in lumbar vertebrae of aging female mice. Calcif Tissue Int. 1990; 46(2):80–93. [PubMed: 2105153]
24. Buhl KM, Jacobs CR, Turner RT, Evans GL, Farrell PA, Donahue HJ. Aged bone displays an increased responsiveness to low-intensity resistance exercise. J Appl Physiol. 2001; 90(4):1359–1364. [PubMed: 11247935]
25. Srinivasan S, Agans SC, King KA, Moy NY, Poliachik SL, Gross TS. Enabling bone formation in the aged skeleton via rest-inserted mechanical loading. Bone. 2003; 33(6):946–955. [PubMed: 14678854]
26. Pruitt LA, Taaffe DR, Marcus R. Effects of a 1 year high-intensity versus low-intensity resistance training program on bone mineral density in older women. J Bone Miner Res. 1995; 10(11):1788–1795. [PubMed: 8592957]
27. Allison SJ, Folland JP, Rennie WJ, Summers GD, Brooke-Wavell K. High impact exercise increased femoral neck bone mineral density in older men: a randomised unilateral intervention. Bone. 2013; 53:321–328. [PubMed: 23291565]
28. Hoffler CE, Hankenson KD, Miller JD, Bilkhu SK, Goldstein SA. Novel explant model to study mechanotransduction and cell-cell communication. J Orthop Res. 2006; 24(8):1687–1698. [PubMed: 16788985]
29. Meganck JA, Kozloff KM, Thornton MM, Broski SM, Goldstein SA. Beam hardening artifacts in micro-computed tomography scanning can be reduced by X-ray beam filtration and the resulting images can be used to accurately measure BMD. Bone. 2009; 45(6):1104–1116. [PubMed: 19651256]
30. Volkman SK, Galecki AT, Burke DT, Paczas MR, Moalli MR, Miller RA, et al. Quantitative trait loci for femoral size and shape in a genetically heterogeneous mouse population. J Bone Miner Res. 2003; 18(8):1497–1505. [PubMed: 12929939]
31. Draper ER, Morris MD, Camacho NP, Matousek P, Towrie M, Parker AW, et al. Novel assessment of bone using time-resolved transcutaneous Raman spectroscopy. J Bone Miner Res. 2005; 20(11): 1968–1972. [PubMed: 16234970]
32. Mazzali M, Kipari T, Ophascharoensuk V, Wesson JA, Johnson R, Hughes J. Osteopontin—a molecule for all seasons. QJM. 2002; 95(1):3–13. [PubMed: 11834767]

33. Cheng MZ, Zaman G, Rawlinson SC, Pitsillides AA, Suswillo RF, Lanyon LE. Enhancement by sex hormones of the osteoregulatory effects of mechanical loading and prostaglandins in explants of rat ulnae. J Bone Miner Res. 1997; 12(9):1424–1430. [PubMed: 9286758]
34. Waldorff EI, Goldstein SA, McCreadie BR. Age-dependent microdamage removal following mechanically induced microdamage in trabecular bone in vivo. Bone. 2007; 40(2):425–432. [PubMed: 17055351]
35. Bonar LC, Roufosse AH, Sabine WK, Grynpas MD, Glimcher MJ. X-ray diffraction studies of the crystallinity of bone mineral in newly synthesized and density fractionated bone. Calcif Tissue Int. 1983; 35(2):202–209. [PubMed: 6850400]
36. Currey JD. Effects of differences in mineralization on the mechanical properties of bone. Philos Trans R Soc Lond B Biol Sci. 1984; 304(1121):509–518. [PubMed: 6142490]
37. Donnelly E, Chen DX, Boskey AL, Baker SP, van der Meulen MC. Contribution of mineral to bone structural behavior and tissue mechanical properties. Calcif Tissue Int. 2010; 87(5):450–460. [PubMed: 20730582]
38. Burr DB. The contribution of the organic matrix to bone's material properties. Bone. 2002; 31(1): 8–11. [PubMed: 12110405]
39. Raghavan M, Sahar ND, Kohn DH, Morris MD. Age-specific profiles of tissue-level composition and mechanical properties in murine cortical bone. Bone. 2012; 50(4):942–953. [PubMed: 22285889]
40. Yerramshetty JS, Akkus O. The associations between mineral crystallinity and the mechanical properties of human cortical bone. Bone. 2008; 42(3):476–482. [PubMed: 18187375]
41. Mehta M, Strube P, Peters A, Perka C, Hutmacher D, Fratzl P, et al. Influences of age and mechanical stability on volume, microstructure, and mineralization of the fracture callus during bone healing: is osteoclast activity the key to age-related impaired healing? Bone. 2010; 47(2): 219–228. [PubMed: 20510391]
42. Joiner DM, Tayim RJ, Kadado A, Goldstein SA. Bone marrow stromal cells from aged male rats have delayed mineralization and reduced response to mechanical stimulation through nitric oxide and ERK1/2 signaling during osteogenic differentiation. Biogerontology. 2012; 13(5):467–478. [PubMed: 22944913]
43. Justesen J, Stenderup K, Eriksen EF, Kassem M. Maintenance of osteoblastic and adipocytic differentiation potential with age and osteoporosis in human marrow stromal cell cultures. Calcif Tissue Int. 2002; 1:36–44. [PubMed: 12200657]
44. Busse B, Djonic D, Milovanovic P, Hahn M, Puschel K, Ritchie RO, et al. Decrease in the osteocyte lacunar density accompanied by hypermineralized lacunar occlusion reveals failure and delay of remodeling in aged human bone. Aging Cell. 2010; 9(6):1065–1075. [PubMed: 20874757]
45. Vashishth D, Verborgt O, Divine G, Schaffler MB, Fyhrie DP. Decline in osteocyte lacunar density in human cortical bone is associated with accumulation of microcracks with age. Bone. 2000; 26(4):375–380. [PubMed: 10719281]
46. Xia X, Batra N, Shi Q, Bonewald LF, Sprague E, Jiang JX. Prostaglandin promotion of osteocyte gap junction function through transcriptional regulation of connexin 43 by glycogen synthase kinase 3/beta-catenin signaling. Mol Cell Biol. 2010; 30(1):206–219. [PubMed: 19841066]

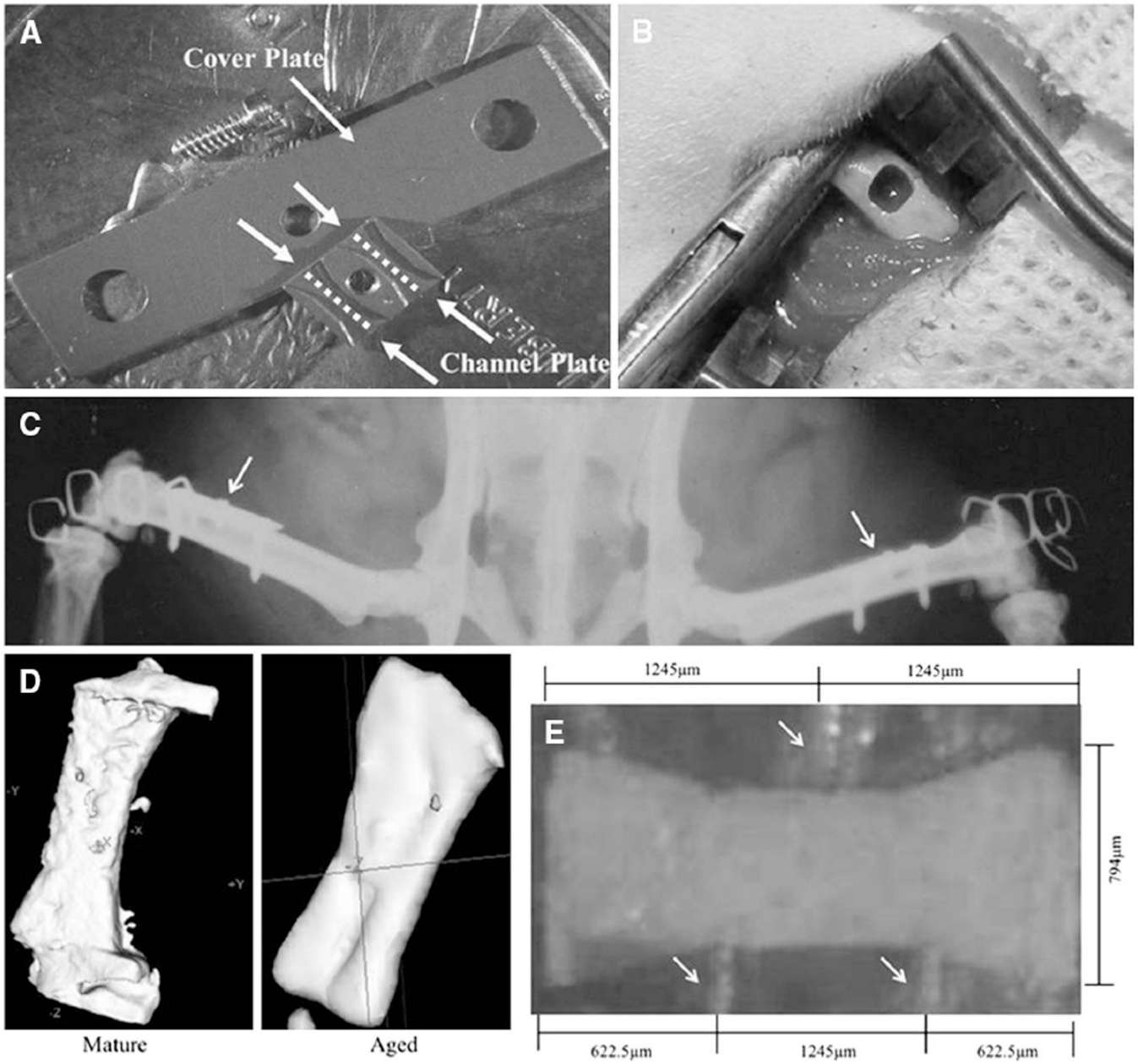

Fig. 1.

a Implant hardware. *Arrows* point to the cover and channel plates. *Dashed lines* illustrate the open parallel channels. **b** Femoral cortical defect. **c** Postoperative radiograph of implanted hardware. *Arrows* point to implants. **d** Three-dimensional microCT reconstructed isosurface of regenerated explants from mature and aged rats. **e** Regenerated explant within the three-point bending device. *Arrows* point to loading supports

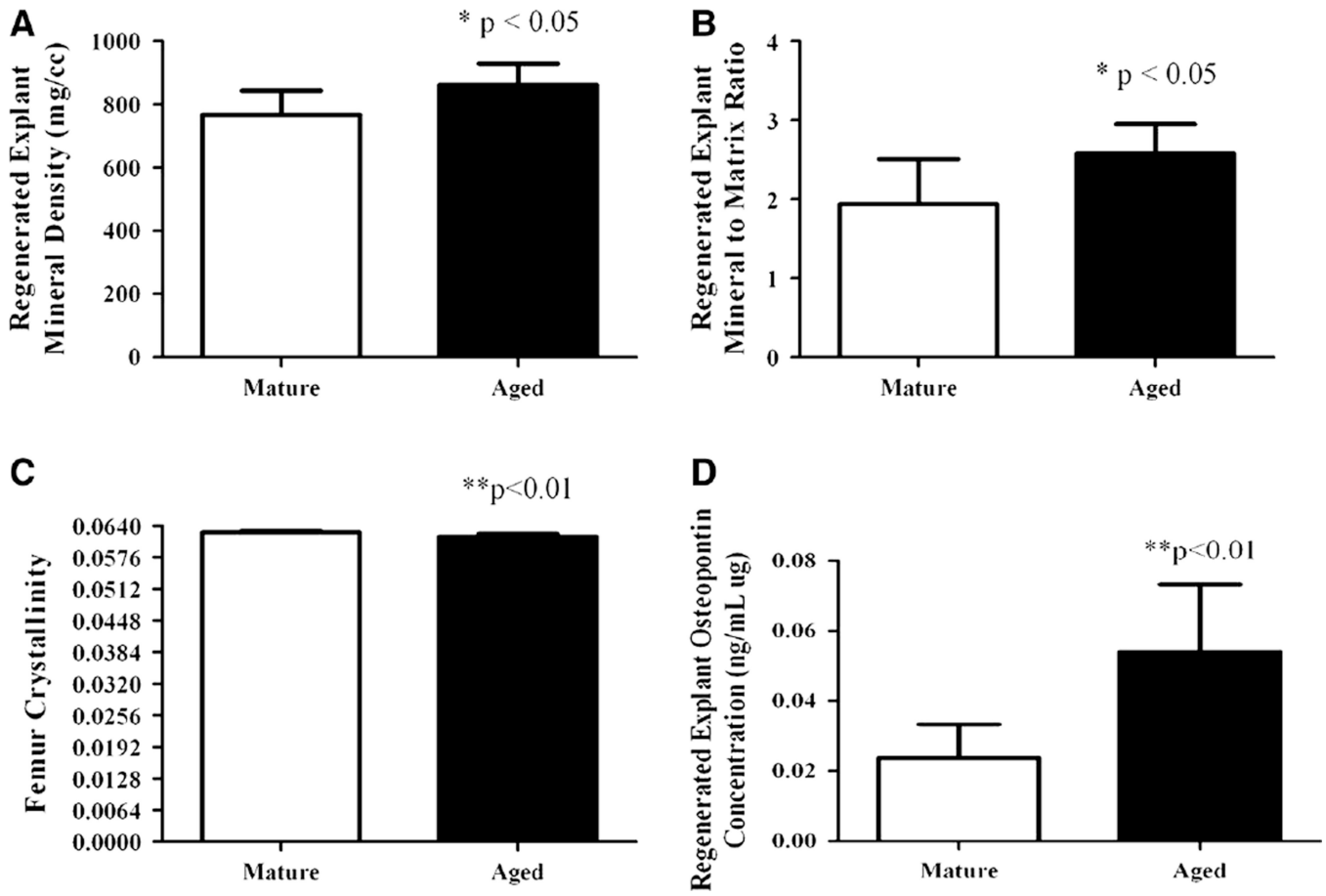

Fig. 2.

a Regenerated explant mineral density expressed as mean ± SD for mature (n = 6) and aged (n = 8) rats; *p <0.05 between groups. **b** Regenerated explant mineral-to-matrix ratio expressed as mean ± SD for mature (n = 6) and aged (n = 8) rats; *p < 0.05 between groups. **c** Femoral cortical bone crystallinity expressed as mean ± SD for mature (n = 10) and aged (n = 10) rats; **p < 0.01 between groups. **d** Regenerated explant secreted osteopontin concentration expressed as mean ± SD for mature (n = 6) and aged (n = 8) rats; **p < 0.01 between groups

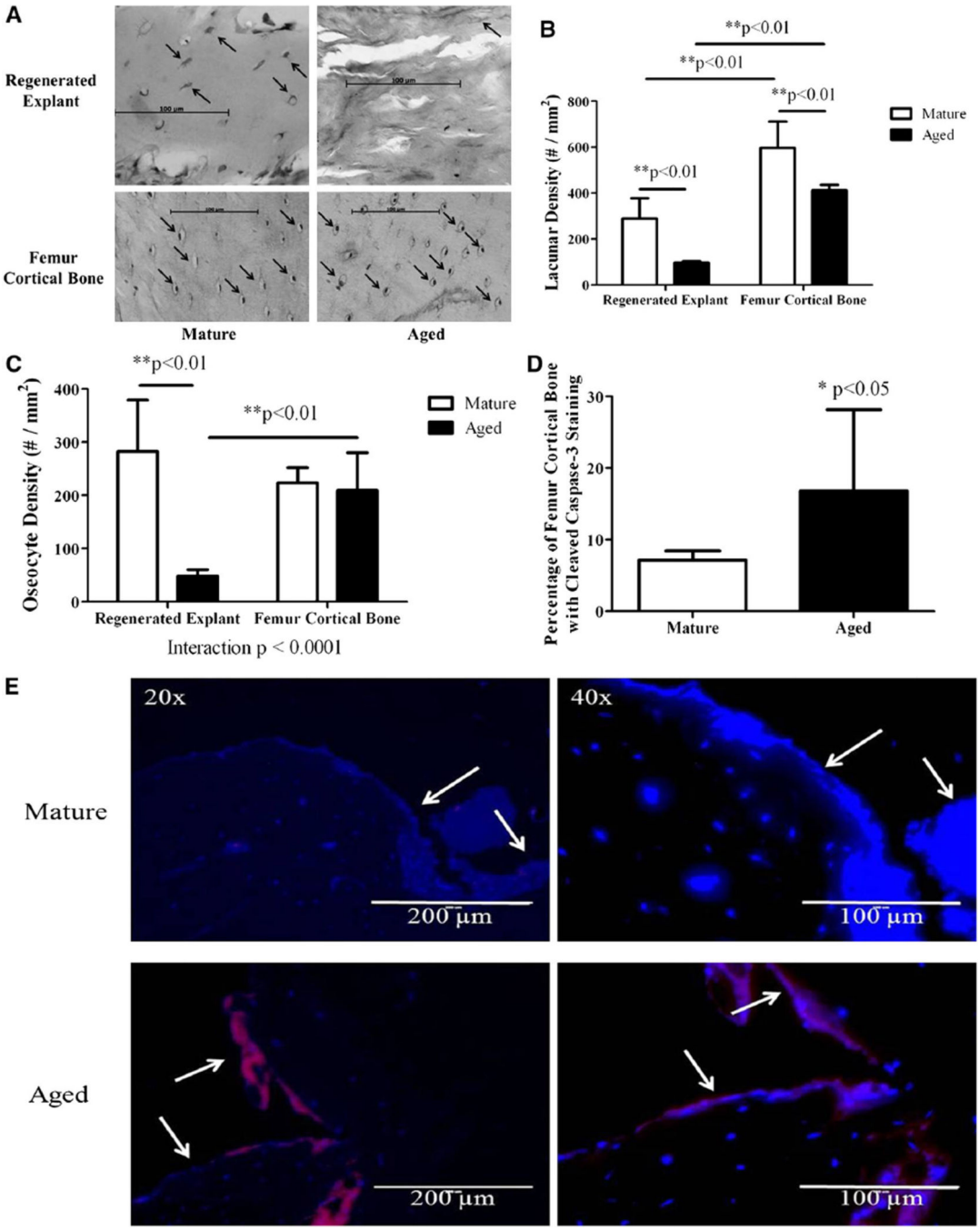

Fig. 3.

a Histological sections of regenerated explants and femoral cortical bone from mature (*n* = 6, 10) and aged (*n* = 8, 10) rats. *Arrows* point to lacunae, some of which contain osteocytes. **b** Lacunar density of regenerated explant sections from mature (*n* = 6) and aged (*n* = 8) rats and of femoral cortical bone from mature (*n* = 10) and aged (*n* = 10) rats expressed as mean ± SD. **c** Osteocyte density of regenerated explant sections from mature (*n* = 6) and aged (*n* = 8) rats and of femoral cortical bone from mature (*n* = 10) and aged (*n* = 10) rats expressed as mean ± SD. **d** Area of cleaved caspase-3 stain normalized to femoral cortical bone area

surrounding the defect (expressed as a percentage) for mature (n = 10) and aged (n = 10) rats expressed as mean ± SD. **e** Cleaved caspase-3 (*red*)- and DAPI (*blue*)-stained sections of femoral cortical bone surrounding the defect from mature (n = 10) and aged (n = 10) rats at ×20 and ×40. *Arrows* point to the edges of the rectangular defect

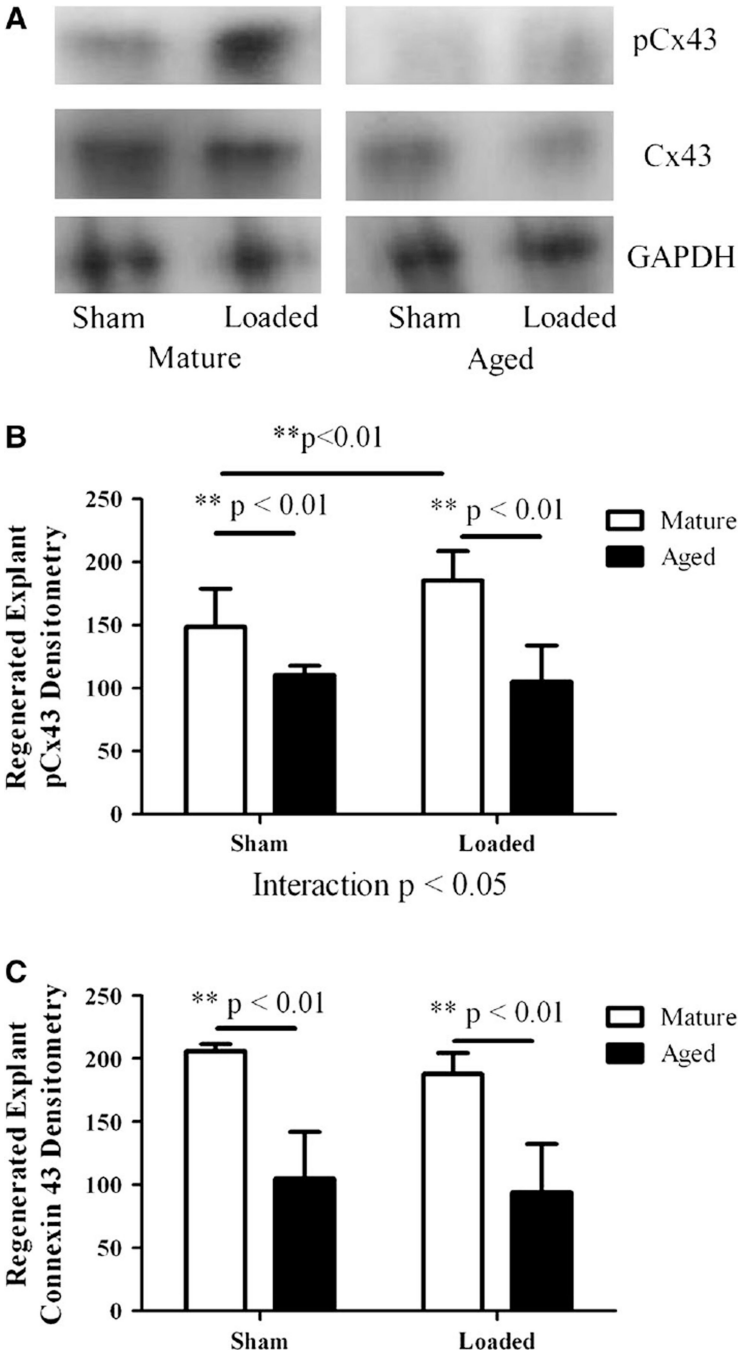

Fig. 4.

For all panels, the numbers of regenerated explants tested were $n = 11$ sham, $n = 11$ loaded for mature rats and $n = 9$ sham, $n = 9$ loaded for aged rats. **a** Western blots of phosphorylated, total Cx43, and GAPDH for sham-treated and loaded regenerated explant specimens from mature and aged animals. **b** Phosphorylated Cx43 densitometry expressed as mean ± SD for sham-treated and loaded regenerated explant specimens from mature and

aged rats. **c** Cx43 densitometry expressed as mean ± SD for regenerated explant specimens from mature and aged rats

Table 1

Femur cortical bone microCT measurements

	Mature	Aged
Cortical BMD (mg/cc)	1,900 ± 8.33	2,300 ± 41.67*
Cortical thickness (mm)	0.09 ± 0.06	0.095 ± 0.13
Cortical cross-sectional area (mm^2)	7.20 ± 0.50	8.1 ± 0.25*
Inner fiber length (mm)	1.10 ± 0.05	1.3 ± 0.03*
Outer fiber length (mm)	1.80 ± 0.08	2.15 ± 0.05*
Bending moment of inertia ($1/m^4$)	7.20 ± 1.05	12.0 ± 1.50*

Values are expressed as mean ± SD

* $p < 0.01$ between age groups

Table 2

Regenerated tissue NO concentration ($\times 10^{-3}$ μM/μg)

Time (min)	Mature sham	Mature loaded	Aged sham	Aged loaded
15	18.4 ± 15.0	29.2 ± 20.9	0.4 ± 0. 5**	1.6 ± 3.5***
30	12.4 ± 7.9	30.5 ± 26.0	0.1 ± 0.3**	1.1 ± 2.5***
45	28.2 ± 27.4	42.9 ± 30.5	4.9 ± 5.7*	0.7 ± 1.6***
60	37.2 ± 33.7	36.6 ± 22.0	6.2 ± 8.9	14.6 ± 22.1

Values are expressed as mean ± SD (n = 11 sham, n = 11 loaded for mature rats and n = 9 sham, n = 9 loaded for aged rats). One extreme outlier NO sample was removed from every group except aged 15 min sham, mature 15 min sham, mature 30 min sham, and mature 60 min sham

* $p < 0.05$ between sham-treated explants from aged animals and loaded explants from mature animals,

** $p < 0.01$ between sham-treated explants from aged animals and loaded explants from mature animals, and

*** $p < 0.01$ between age groups for loaded explants

Table 3

Regenerated tissue PGE_2 concentration ($\times 10^{-9}$)

Time (min)	Mature sham	Mature loaded	Aged sham	Aged loaded
15	12 ± 7	35 ± 49	28 ± 19	28 ± 19
30	13 ± 5	30 ± 34	19 ± 23	12 ± 13
45	8 ± 8	12 ± 9	13 ± 8	9±5
60	8 ± 3	69 ± 71*	17 ± 9	10 ± 6

Values are expressed as mean ± SD (n = 11 sham, n = 11 loaded for mature rats and n = 9 sham, n = 9 loaded for aged rats). One extreme outlier PGE_2 sample was removed from the aged 30 and 60 min loaded, mature 15 min sham, and mature 45 min loaded groups. Two extreme outlier PGE_2 samples were removed from the aged 30, 45, and 60 min sham groups

* $p < 0.05$ between sham-treated and loaded explants from mature animals